Chapter 21
Very high frequency coastal acoustics

T. G. LEIGHTON
University of Southampton, UK

G. J. HEALD
DSTL, UK

Summary

Higher frequencies provide us with the short wavelengths required to resolve the small features which provide much of the fascination of coastal waters, be they objects in or on the seabed (sand ripples, weed, shells, wreckage, military ordinance), sub-bottom features (geology, pipelines), or oceanographically significant entities in the water column (fauna, flora, suspended solids, bubbles). High frequency signals also provide us with the temporal resolution required to follow the rapid fluctuations which characterize many of these important oceanographic features. For example a breaking wave in the surf zone, along with its associated turbulence and currents, can dramatically alter the shallow water oceanography in under a second.

This chapter will discuss a scenario which is doubly unsolved, first because the environment will be coastal waters (which represent perhaps the least cataloged regions of the ocean) and, second, because the sensors will involve Very High Frequency (VHF) acoustics. For the purposes of this work, it is convenient to define VHF as 200 kHz and higher. Not only is this lower limit (200 kHz) greater than the frequencies used by the majority of underwater acoustic sensors, but it is also close to the boundary between the "known" and "unknown" in a number of applications.

Contents

© H. Medwin 2005

21.1 Introduction

It is ironic that the region of sea most close to us geographically should be one of the least explored acoustically. The main reasons for this are two-fold. First, in the Cold War period the emphasis was on deep water acoustics, primarily for the detection of nuclear submarines. This has changed since the fall of the Berlin Wall, when the likely arena for operation has been shallow water coastal areas. Second, the science of acoustics is very difficult to apply in near-shore (or "littoral") regions, where propagation is complicated not only by multiple reflections from the air/sea interface and the bottom, but also by the myriad acoustically active fluctuating inhomogeneities which are present in the water column in coastal waters.

In such waters there is a tendency to use higher frequencies. Consider, for example, that a 3 m separation between the top and bottom of the water column corresponds to a propagation time of around 2 ms. This not only means that 1 s of acoustic testing may incorporate hundreds of reflections. It also illustrates one of the reasons why coastal acoustics tend to exploit higher frequencies: whilst that 2 ms interval corresponds to only 1/5 of the cycle at 100 Hz, it corresponds to 200 cycles at 100 kHz. There are therefore many more cycles available for transmitting information. High frequencies also allow pulse lengths to be shortened, offering a reduction in the complicated multipath reverberation. Those multipaths which remain are more likely to be clearly resolved, because the same number of cycles at high frequency covers a much smaller spatial range in the water than it does at low frequencies. Once resolved, multipaths and target interactions can be used to gain information about the environment.

Such apparent advantages may, however, be complicated or compromised by acoustic absorption, which increases with frequency (see Section 2.4.2). Whilst higher absorption might reduce the number of multipaths in the received signal, it will also reduce detection ranges. Then again, high absorption might be seen not just as a problem which limits signal range, but absorption itself might be the measure by which we monitor the ocean environment. Examples are given in Sections 21.4–21.6, where for example the highest frequencies can be so strongly absorbed in sediment that reflections from the seabed can primarily contain

information from the seabed/water interface, a fact which can be exploited in their interpretation.

Higher frequencies also are further removed from some of the sources of ambient noise in coastal regions (see Section 5.5). One has only to swim through the surf to appreciate the level of noise from wave-breaking and saltation in the surf zone, as well as non-acoustic sources of audible or hydrophone "noise" such as turbulence; and from there to swim out over a reef and hear biological activity, and the noise from such human activities as industry and shipping. With some exceptions, many of these would not produce very high frequencies at source, and of course absorption during propagation will further reduce their high frequency contribution to the signal at a remote detector.

At the start of this chapter, 200 kHz was deemed to be close to the boundary between the "known" and "unknown" in a number of applications. Taking two examples which will be explored in the chapter, the models for acoustical scattering from sediment are only validated at lower frequencies (Section 21.5); and measurements of bubbles in coastal waters have been restricted to those having resonance frequencies lower than about 200 kHz (Section 21.6). Because the VHF frequency range is relatively unexplored in the ocean, this chapter is written from an acoustical point of view, rather than an oceanographic one, in which information can be derived from well-characterized acoustical tools.

The use of high frequencies brings with it a set of problems not encountered with the lower frequencies which are more often used in oceanography. Because the signal is absorbed to a far greater extent, transducers are required which can generate high amplitude fields. As a result, consideration must be given to the potential for non-linearities in both source and propagation (see Chapter 4). The complexity of the environment, with its small scale features and rapid fluctuations, has stimulated exploration of signal features (bandwidth, coherence) which have placed further requirements on the transducer design, signal processing, and understanding of the acoustics. These issues are explored in the rest of chapter.

21.2 Acoustics

Restating the development in Section 4.1, the characterization of the propagation of an acoustic wave in a fluid requires three fundamental inputs enshrined in equations reflecting: first, the motion of mass in a fluid; second, the fluid dynamic properties relating such motions to the pressure gradient which causes them; and third, an equation which shows that pressure gradient to be part of a longitudinal wave. Stated in one-dimensional form, these three equations are, respectively: the equation

of continuity

$$\frac{\partial \rho}{\partial t} + \frac{\partial (\rho v)}{\partial x} = 0 \tag{21.1}$$

where v is the particle velocity, and ρ the fluid density; Euler's equation for an inviscid fluid

$$v\frac{\partial v}{\partial x} + \frac{\partial v}{\partial t} = -\frac{1}{\rho}\frac{\partial p}{\partial x} \tag{21.2}$$

where p is the sum of all steady and unsteady (assumed here to be purely acoustic) pressures; and the wavespeed equation

$$c^2 = \frac{\partial p}{\partial \rho} \tag{21.3a}$$

Combination of these three equations allows formulation of the propagation of acoustic longitudinal waves in a fluid, linearization allowing the generation of what is generally termed the (linearized) plane wave equation. In the small amplitude regime where this is applicable, the sound speed is represented by the phase speed in the linear limit c_0, and the approximation made that $\rho^{-1} \approx \rho_0^{-1}$ where ρ_0 is the equilibrium density. In this linear limit (21.3a) gives

$$c_0^2\frac{\partial \rho}{\partial t} = \frac{\partial p}{\partial t} \qquad c_0^2\frac{\partial \rho}{\partial x} = \frac{\partial p}{\partial x} \tag{21.3b}$$

and substitution of (21.3b) into (21.1) converts the term $(\partial\rho/\partial t)/\rho$ into $(\partial p/\partial t)/(\rho_0 c_0^2)$ to give:

$$\frac{\partial v}{\partial x} + \frac{v}{\rho_0}\frac{\partial \rho}{\partial x} = -\frac{1}{\rho_0 c_0^2}\frac{\partial p}{\partial t} \tag{21.4a}$$

Similarly, if $\rho^{-1} \approx \rho_0^{-1}$ then Euler's equation (21.2) becomes:

$$v\frac{\partial v}{\partial x} + \frac{\partial v}{\partial t} = -\frac{1}{\rho_0}\frac{\partial p}{\partial x} \tag{21.4b}$$

Linear acoustics is based on the assumption that two of the terms in the above series of equations are negligible, specifically that $|(v/\rho_0)(\partial\rho/\partial x)| \ll |\partial v/\partial x|$ when calculating $(\partial p/\partial t)/(\rho_0 c_0^2)$ using (21.4a); and that $|v(\partial v/\partial x)| \ll |\partial v/\partial t|$ when calculating $(\partial p/\partial x)/\rho_0$ using (21.4b). Differentiation of (21.4a) with respect to t, and of (21.4b) with respect to x, gives the one-dimensional linearized plane wave equation for pressure if the equivalence $(\partial^2 v/\partial x\partial t) = (\partial^2 v/\partial t\partial x)$ is made:

$$\frac{\partial^2 p}{\partial t^2} = c_0^2\frac{\partial^2 p}{\partial x^2} \tag{21.5}$$

Equation (21.5) describes a linear pressure wave propagating at speed c_0, and has solutions $p = g(t \pm x/c_0)$. Similarly differentiation of (21.4a) with respect to x, and of (21.4b) with respect to t, with the same two terms deemed to be negligible, gives the one-dimensional linearized plane wave

equation for particle velocity, with solutions $v = f(t \pm x/c_0)/(\rho_0 c_0)$, since

$$\frac{\partial v}{\partial t} = \frac{f'}{\rho_0 c_0} \qquad \frac{\partial^2 v}{\partial t^2} = \frac{f''}{\rho_0 c_0} \qquad \frac{\partial v}{\partial x} = \pm\frac{f'}{\rho_0 c_0^2}$$
$$\frac{\partial^2 v}{\partial x^2} = \frac{f''}{\rho_0 c_0^3} \quad \text{satisfy} \quad \frac{\partial^2 v}{\partial t^2} = c_0^2 \frac{\partial^2 v}{\partial x^2} \tag{21.6}$$

where $f' = \partial f/\partial(t \pm x/c_0)$. If such linear solutions are valid, then the conditions which make them valid (i.e., which ensure $|v\,(\partial v/\partial x)| \ll |\partial v/\partial t|$ and $|(v/\rho_0)\,(\partial \rho/\partial x)| \ll |\partial v/\partial x|$) are readily found. Taking the first inequality, $|v\,(\partial v/\partial x)| \ll |\partial v/\partial t|$, substitution from (21.6) gives

$$v\frac{\partial v}{\partial x}\Big/\frac{\partial v}{\partial t} = \pm\frac{v}{c_0} \tag{21.7a}$$

Consider the second inequality, $\left|(v/\rho_0)\left(\partial\rho/\partial x\right)\right| \ll \left|\partial v/\partial x\right|$ in the same linear limit, where (21.3b) is valid. Since neglect of the non-linear term in (21.4b) implies $\partial v/\partial t = (-\partial p/\partial x)/\rho_0$, then substitution from (21.6) reduces the second ratio to

$$\frac{v}{\rho_o}\frac{\partial \rho}{\partial x}\Big/\frac{\partial v}{\partial x} = -\frac{v}{c_0^2}\frac{\partial v}{\partial t}\Big/\frac{\partial v}{\partial x} = \pm\frac{v}{c_0} \tag{21.7b}$$

Hence the linear limit is approached as the acoustic Mach number becomes small and the two non-linear terms become negligible (see Section 1.6.2). As stated in the introduction, when VHF ($\gtrsim$200 kHz) acoustics are used in coastal waters, both the increased absorption seen at higher frequencies, and the extra losses due to absorption and scattering by inhomogeneities, mean that to obtain a good signal-to-noise ratio, the tendency is to use high amplitude signals at the source.

The consequence of finite acoustic Mach numbers is that (21.5) no longer holds, and a waveform which is initially sinusoidal will not remain so because of two non-linear effects which act co-operatively. Both can be readily understood through the realization that, if dissipation is small, then p and v would be in phase (Leighton, 1994). First, there is a *convection* effect. In simple terms, if v/c is not negligible, then parts of the wave tend to propagate as $c + v$. The particle velocity varies throughout the wave, and so the greater the local acoustic pressure, the greater the velocity of migration of that section of the wave. If then p and v are in phase, regions of compression (where the v and c are in the same direction) would tend to migrate faster than the regions of rarefaction (where v is opposite to c). The pressure peak travels with the greatest speed, the trough with the least (see Fig. 4.2).

Second, there is an effect which arises because, when a fluid is compressed, its bulk modulus and stiffness increase. This results in an increase in sound speed, and this effect too will cause the pressure peaks

to travel at greater speed than the troughs, and tend to try to catch up and encroach upon them. See also Section 4.1.

A continuous wave that is initially sinusoidal will therefore distort in the way shown in Figure 21.1. The plots in *(i)* illustrate the time history of the wave, measured at increasing distances (*a–f*) from the source. The corresponding spectra are shown in *(ii)*. Close to source, the waveform is initially nearly sinusoidal (*a(i)*) and single frequency (*a(ii)*). As it propagates through the medium, each compressive region gains upon the preceding rarefactive half-cycle, the peak positive acoustic pressure appearing earlier and earlier in the time history compared to the peak rarefaction. An accumulated steepness of the waveform between the two develops (*b(i)*) and harmonics appear in the spectrum (*b(ii)*). After propagating a certain distance (the *discontinuity length*) the waveform includes a discontinuity: a shock wave develops (*c(i)*), with an associated continuum in the spectrum visible between the harmonic peaks (*c(ii)*). The contribution of higher harmonics to the waveform is clearly visible (*c(i)*). Note that the amplitude after this time decreases, because any further compressional advance leads to dissipation and results in a reduction in the amplitude of the shock. This is because the waveform distortion has been equivalent to transferring some of the energy of the initial wave to higher frequencies, which are more strongly absorbed (*d*, *e*). The energy transfer is not sufficient to maintain the shock, and the wave approaches a low-amplitude sinusoidal form (termed "old age") (*f*).

Hence during non-linear propagation energy is pumped from lower to higher frequencies, where it is preferentially absorbed. This means that the net attenuation over distance will be greater if non-linear propagation occurs, than if conditions were linear. Furthermore, a narrow band detector tuned to the frequency of the emitted pulse might fail to detect energy in the returned signal which is outside of its bandwidth (and hence "invisible" to it). Both of these will act to reduce the signal-to-noise of the received signal, a problem which may not be alleviated by simply increasing the amplitude of the emitted pulse (since this enhances the non-linear effects, a phenomenon known as "acoustic saturation" see Leighton (1998) and Chapter 4).

Propagation such as that described above is just one of the possible sources of non-linearity: others include the transducer itself, and entities within the water column (see Section 21.6). The degree to which the effects occur for a given acoustic signal in the coastal environment of course depends not only on the non-linearity (and hence the rate at which energy is transferred from lower to higher frequencies) but also on the absorption. Some coastal features, such as bubbles, increase both, and it may be that the absorption is so great that non-linearity is not present

a(i)

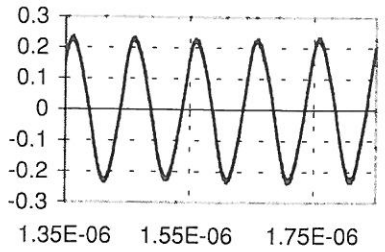

a(ii)

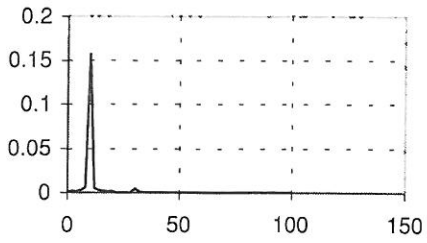

b(i)

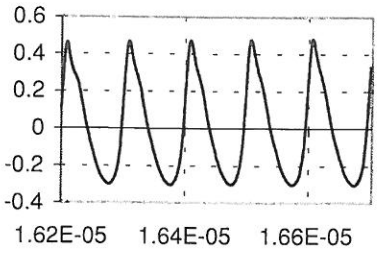

b(ii)

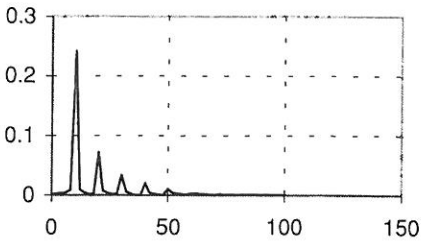

c(i)

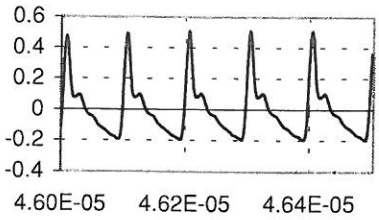

c(ii)

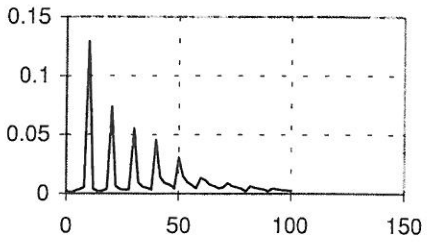

d(i)

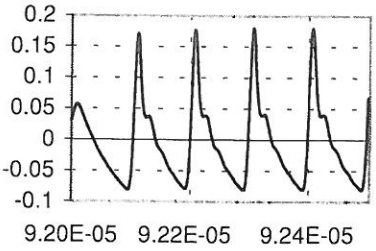

d(ii)

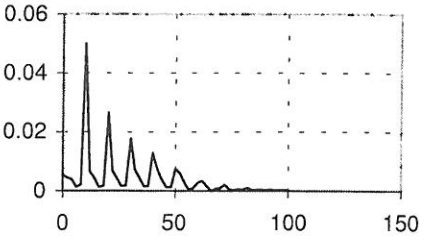

e(i)

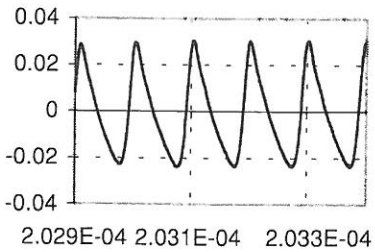

e(ii)

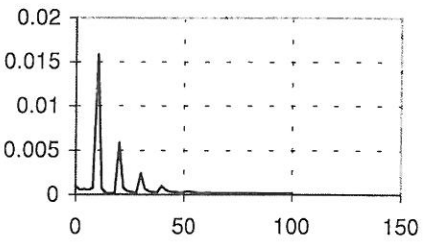

f(i)

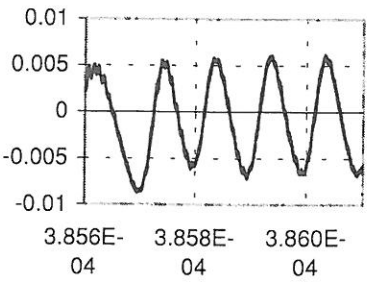

f(ii)

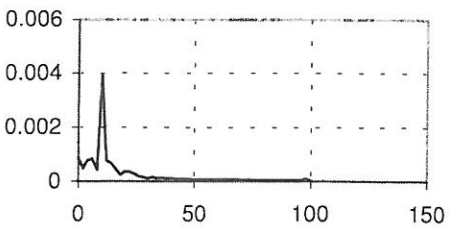

Fig. 21.1

in the received signal. However its possibility during propagation must be appreciated. This is not only because non-linear propagation might cause enhanced absorption, or may make some energy in the received signal "invisible" if it is outside the bandwidth of the detector, but also because it might be exploited. The ability of the propagating medium to generate multiple frequencies, as illustrated in Fig. 21.1, could not only be used to diagnose the properties of that medium (e.g., bubble water). It could also be used to generate a signal containing harmonics across a wide frequency range for simultaneous testing of, say, the scatter from the seabed or a target across a wide range of frequencies (the propagation after scattering, being of lower amplitude, would tend to be linear and so preserve the frequency characteristics of the target within the usual linear constraints of absorption, etc.).

A simple model for the transferring of some energy from lower to higher frequencies (which does not include the critical absorption component) can be found in a simple power series expansion relating, for example, the response ¥(t) of a fluid element to pressure,

$$¥(t) = s_0 + s_1 \cdot p(t) + s_2 \cdot p^2(t) + s_3 \cdot p^3(t) + s_4 \cdot p^4(t) + \ldots \qquad (21.8)$$

where s_0 etc. are coefficients in the expansion. This is adequate to demonstrate the generation of harmonics through a non-linear process (including propagation). If the non-linear fluid element (in this case the liquid) is subjected to single-frequency insonification $p \propto \cos \omega t$, then the second and third harmonics are generated by the quadratic s_2 and cubic s_3 terms, and so on:

$$\begin{aligned} 2\cos^2 \omega t &= 1 + \cos 2\omega t \\ 4\cos^3 \omega t &= \cos 3\omega t + 3\cos 3\omega t \end{aligned} \qquad (21.9)$$

Fig. 21.1. The signal from a 0.25" diameter Panametrics plane transducer, driven by a 10-cycle 10 MHz tone burst. Part (i) (left column) shows the oscilloscope voltage (V) against the timebase (s). The overall system sensitivity (hydrophone plus amplifier, minus loading correction) at 10 MHz was 378.65 nV/Pa, so the peak positive pressures are around 1.2 MPa. Part (ii) (right column) shows the amplitude spectral level against frequency (MHz). Measurements were made with a 2 × 9 micron bilaminar membrane hydrophone (Marconi, with a high gain 100 MHz bandwidth preamplifier). This had an active element of diameter 0.5 mm, separated from the transducer face by (*a*) 2 mm, (*b*) 24 mm, (*c*) 68 mm (the position of the last axial maximum, i.e., the ratio of the square of the faceplate radius to the acoustic wavelength), (*d*) 136 mm, (*e*) 300 mm, (*f*) 570 mm, determined from the time relative to the transducer firing. Data was recorded by a Tektronix TDS 784D DPO oscilloscope (50 ns/div, 5000 point waveforms). The experimental system was aligned according to IEC 61102 prior to measurement: the water temperature was 18.7 °C. (Measurements taken specifically for this chapter by M. Hodnett and B. Zeqiri, National Physical Laboratory, UK.)

Note also that a non-linear element in the sea which is insonified by two coherent frequencies $p(t) = p_1 \cos \omega_1 t + p_2 \cos \omega_2 t$, can generate combination-frequency signals at $\omega_1 \pm \omega_2$, $\omega_1 \pm 2\omega_2$, $\omega_1 \pm 3\omega_2$ etc. since the quadratic term alone gives $2p_2p_1 \cos \omega_1 t . \cos \omega_2 t = p_2p_1\{\cos(\omega_1 + \omega_2)t + \cos(\omega_2 - \omega_1)t\}$.

Whilst this scheme allows an easy appreciation of how harmonics come to be generated during non-linear propagation of high-amplitude acoustic beams through water, and for the operation of parametric sonar devices (Ostrovsky *et al.*, 2003), it is important to recognize that the above scheme is general. As such, any non-linear system can generate such signals, and this can include turbulence and bubbles (Section 21.6), and transducers, the topic of the next section.

21.3 Transducers and signals

The possibility of non-linear propagation is one of the reasons why VHF technology has moved towards the use of wideband transducers. Given that high output powers are required to counteract the acoustic losses at VHF, the use of transducers with high-quality factors would suggest itself. With these, the available energy would be concentrated in a narrow bandwidth, so that high amplitude signals could be projected at specific frequencies. From the preceding section, this has the clear disadvantage that some energy in the returned signal may not be detected if narrowband receivers, or assumptions of linearity, are used.

At low frequencies it is possible to form arrays using individual transducers at an appropriate spacing. Designers generally aim to have the individual element spacing set to less that half the wavelength of the highest frequency so that they can be electronically steered without the introduction of diffraction grating lobes. Half wavelength spacing is only a requirement if steering from broadside to 90° is required. If only smaller steer angles are required, then clearly the separation criterion can be relaxed. At very high frequencies it becomes difficult to produce arrays using individual transducers as the elements, so novel approaches are required.

One of the recent developments in the production of high frequency arrays has been the advent of the 1–3 composite transducers. Rather than using individual transducers as the elements, these arrays are formed from a single block of ceramic. There are two methods used in the production of these arrays, specifically by dicing the ceramic or injection moulding. In dicing, the ceramic is first cut to rods of length equal to a quarter of the wavelength of the desired center frequency. It is then diced, leaving a series of rods that are all cut to the same length, and hence are responsive to a characteristic wavelength. As these arrays are generally

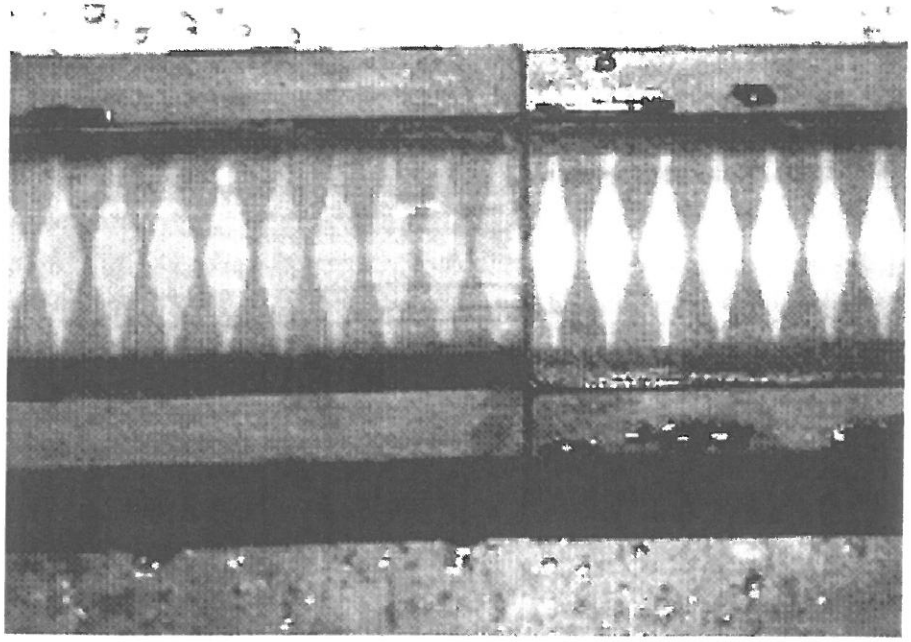

Fig. 21.2. Photograph of a ~20 cm length of a 1–3 composite array showing the ceramic/epoxy grid (fine texture between diamonds) and the shaped elements (the raised cosine function giving them a diamond-like shape in the image), which provide mechanical shading and reduce the vertical sidelobes.

used for wideband signals, the choice of bonding material between each of the rods can be used to adjust the stiffness (and hence the damping coefficient). It is now commonplace to see high frequency arrays with a quality factor of 2 or less. The material used is generally an epoxy resin which has the advantage that once it has set, it keeps the individual rods at a fixed separation.

Having formed a matrix of rods, individual array elements may then be formed by screen printing conductive paint on the front and back of the array. In the simplest case the shape of the element can be made square or rectangular with only a small insulation gap between adjacent elements. In shallow water applications it is often desirable to reduce the scattering from the ocean boundaries. The shape of the element may therefore be tailored to reduce the vertical sidelobes and hence provide vertical shading (Stansfield, 1990). The example given in Fig. 21.2 shows a receiver array where a cosine shading has been applied to the element shape. Owing to the small size of high frequency arrays, it is possible to gather acoustic data from the individual elements. This allows the raw data from each element to be stored for later processing (beamsteering and beamforming) if required.

There are a number of ways that the array can be used to produce and receive broadband signals. In theory it should be possible to produce an impulse in the water, and by taking the Fourier transform to display the spectral content of the received signal. There are a number of reasons why this is not practical. Imperfections in the array mean that achieving perfect matching is not possible, and as a result the overall bandwidth of the array will have a finite limit. Using an impulse would mean that

large amounts of power would be required, in a short space of time, and the commensurate emitter amplitudes would generally be above the cavitation limit of the transducers, resulting in low efficiency.

An additional factor of very high frequency arrays is the range to the near-field/far-field transition. If we use l^2/λ as the criterion (where l is the array length and λ is the acoustic wavelength) then a 1 m array would have a near-field region out to 133 m at 200 kHz, and to 667 m at 1 MHz. Bearing in mind the higher absorption that occurs as the frequency increases, it is possible that all the useful ranges at very high frequencies would be in the near-field. This leaves the sonar designer with two options: either correct for the near-field curvature using Fresnel correction/focusing; or use a shorter array which will result in wider beamwidths and loss of angular resolution.

Prior to the introduction of wideband signals into underwater acoustics, systems were generally limited to pulse transmissions that were modulated with a single frequency (CW). The resolution of these sonars was limited by the minimum pulse length used. A more practical solution to achieve a wideband system is to spread the frequency information over time to produce a time/frequency chirp. High spatial resolution can be achieved by passing the received wideband signal through a replica correlator (Lynn, 1985) so that pulse compression is achieved. The function of a simple finite correlator function may be written as:

$$r_{xy}(t_d) = \int_{-\infty}^{\infty} f_1(t) \cdot f_2(t + t_d) \cdot dt \qquad (21.10)$$

where $f_1(t)$ is the amplitude function of the source signal, $f_2(t)$ is the received signal and t_d represents the time shift between the transmit and receive functions.

At high frequencies the coherence of the received signal is likely to become degraded owing to a number of factors. The small wavelength means that the minor disturbances due to the water column or the ocean boundaries can have a significant impact on the signal. A small roughness on the seabed or the ocean surface will mean that the signal can become incoherent. The shape of the wavefront can be affected by spatial or temporal variability, turbulence, moving waves, scintillation, or sediment in transport, and this can limit the ability to beamform over the full array. At lower frequencies attempts have been made to overcome wavefront distortion by using time reversal or phase conjugation techniques (Edelmann *et al.*, 2002). These methods rely on a point source so that the time of flight to each element along an array can be stored. Using reciprocity, the array can then be used to transmit a signal with the same time (or phase) delays introduced. By definition this means

that there will be a focal point where the original source was located, provided that the environment has remained stationary. This type of technique originated in focusing for medical transducers, and so it has been applied in laboratory and biomedical environments at the VHF frequencies of interest in this chapter. The authors are not aware of any coastal water experiments in time reversal or phase conjugation that have been reported using VHF acoustics (Kustov *et al.* (1985) exploited signals of 60 and 100 kHz in a laboratory pool). Because the environment must be stable over the timescale between the point source transmission and the reception back at that point, it is possible that coastal waters may not be stable enough to show any improvement when VHF time reversal or phase conjugation techniques are attempted. The environmental factors presented in the remainder of this chapter cover some of the issues that will impact on the coherence, distortion, and attenuation of VHF acoustic signals. This is a relatively new area of ocean acoustics so there is still much research that is required.

A wideband facility opens up other opportunities, however. Acoustical oceanography differs from active sonar in that the sources of signal loss which hindered target detection in sonar might be the very oceanographic features which, in acoustical oceanography, one is trying to observe. Sections 21.5 and 21.6 detail how scattering from inhomogeneities in the water column can be used to diagnose the nature of those inhomogeneities: in target detection by active sonar, such oceanographic scattering would simply be viewed as a signal loss which one would try to avoid; in acoustical oceanography that "loss" is the signal itself. Similarly, whilst the temptation is to view the introduction of non-linearity as a problem, it can in fact be exploited: Section 21.6 shows how the non-linearity itself can be used to diagnose the bubble population. Before that however, we will consider the bottom of the water column, and work upwards, beginning with the measurement of bottom properties.

21.4 The seabed

The increase in attenuation with increasing frequency is a characteristic, not just of sea water, but also of the seabed. When an acoustic signal is scattered from the sea floor, some of the energy returns from the seabed/water column interface (the "top" of the seabed) and some is reflected from regions beneath the sea floor. Therefore, the use of VHF acoustics opens up the possibility of emphasizing scattering from the top of the seabed, since the energy which propagated the greater depths will be that much reduced. In addition, with a reduction in wavelength comes the ability to resolve fine detail on the sea floor, such as sand ripples, shells, and other fauna and flora (Williams *et al.*, 2001).

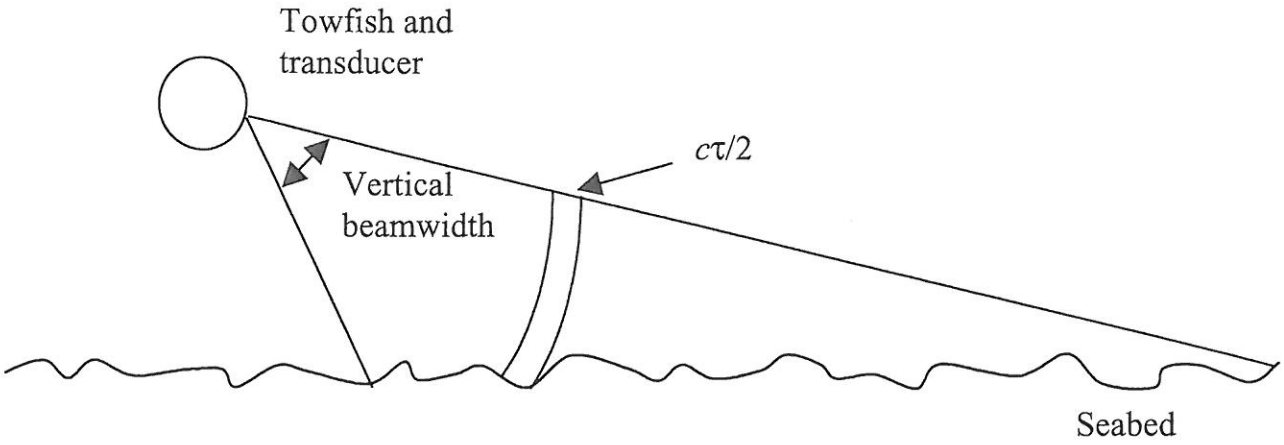

Fig. 21.3. Schematic of sidescan sonar geometry (single side), where c is the sound speed and τ is the pulse duration.

High frequency seabed acoustic systems have been employed for a number of decades through the application of sidescan sonar (Fig. 21.3). These sonars are generally housed in a towed body and are "flown" relatively close to the seabed, and the transducer axis is perpendicular to the forward motion of the host platform. The acoustic beam is incident on the seabed at a low grazing angle. This means that the undulations due to the sediment roughness have high intensities on the facing slopes, but the backslopes of the ripples are in an acoustic shadow. As the sonar moves through the water, pings emitted at regular intervals are used to build up a 2D image of the seafloor features. Figure 21.4 shows an output from a 325 kHz sidescan sonar from a region where patches of different sediment can be seen in the different bedform texture of various parts of the image. Where the parameters of the sonar and geometry are well known, it is possible to use image texture processing algorithms to discriminate the regions of different sediment type. With ground truth information, it is then possible to provide aided classification of the seabed (Fig. 21.5).

Commercial sidescan sonars are available covering the frequency range from about 100 kHz, for wide swath widths, up to about 600 kHz. At these higher frequencies the range is significantly reduced, but fine resolution can be obtained in images of the sea floor, and of objects on or in it. With the advent of unmanned underwater vehicles, it is anticipated that the upper frequency limit may move even higher (although issues regarding coherence and platform stability may prove to be a limiting factor).

Treating the seabed backscatter as an image tends to ignore the physical processes of the actual sea floor scattering that are taking place. It also does not take account of the image sensitivity to other changes in the

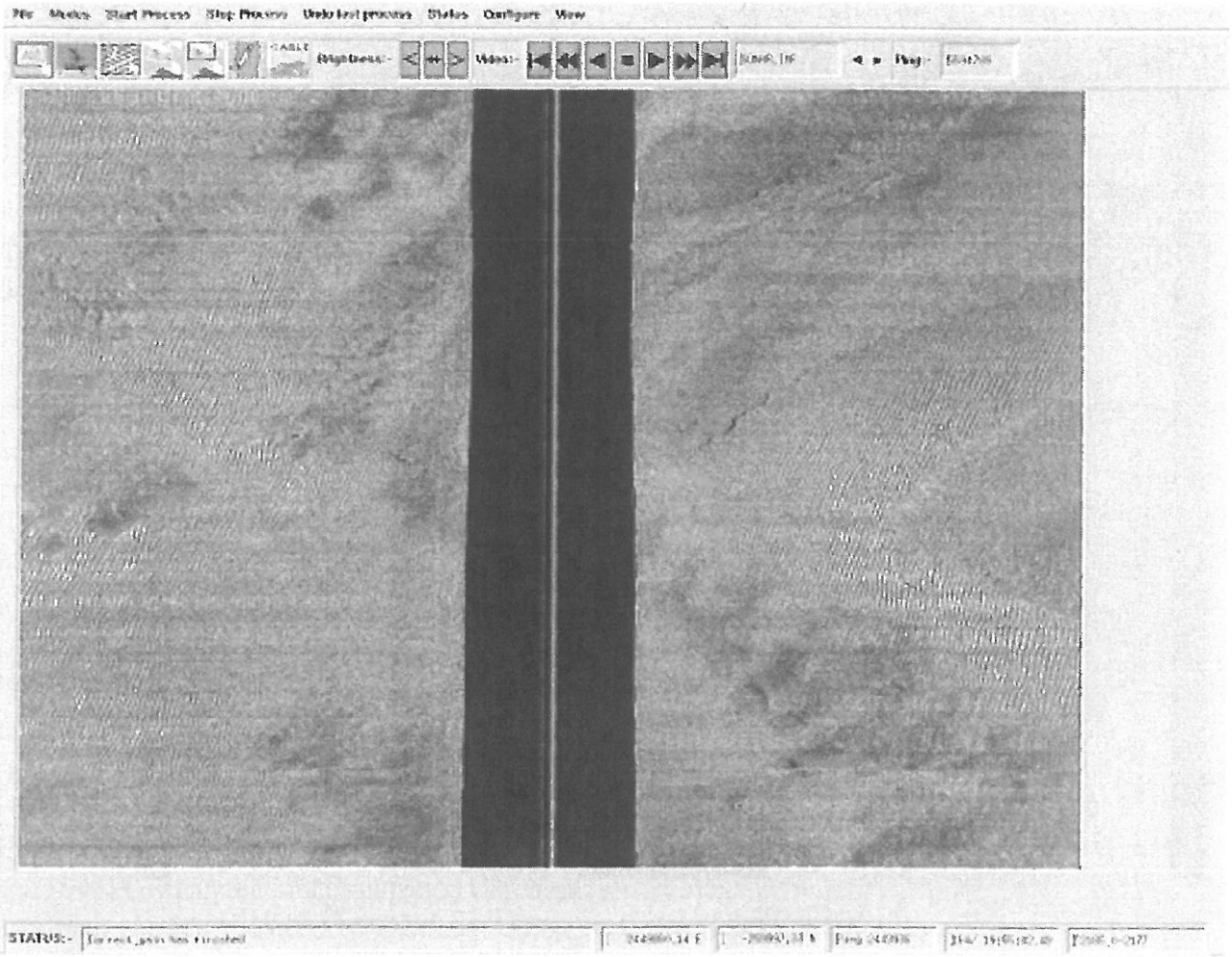

Fig. 21.4. A 325 kHz sidescan sonar seabed image. The left panel corresponds to 100 m (swath width) of seabed to the left of the towfish, and the right panel corresponds to the 100 m swath width to the right. (Image provided using the Classiphi™ system courtesy of QinetiQ Ltd.)

environment, or in the system being used to gather the data. It is clear that very few publications have included the physics of sea floor scattering in the frequency range above 200 kHz, and current high frequency sediment scattering models have only been validated up to about 150 kHz.

The concept of seabed "roughness" (as exploited in the classification scheme of Fig. 21.5) is no simple matter. Physically, there is of course the morphology or "surface relief," which can take an anisotropic 2D form over the seabed, but for which a simple example is a uniform set of 1D seabed ripples. In addition to this, there is the roughness imparted by the individual grains, the largest of which is gravel (of which there are four categories based on the range of particle diameters, $2a$: boulders $2a > 256$ mm; cobbles 256 mm $> 2a > 64$ mm; pebbles 64 mm $> 2a > 4$ mm; granules 4 mm $> 2a > 2$ mm). Smaller grains

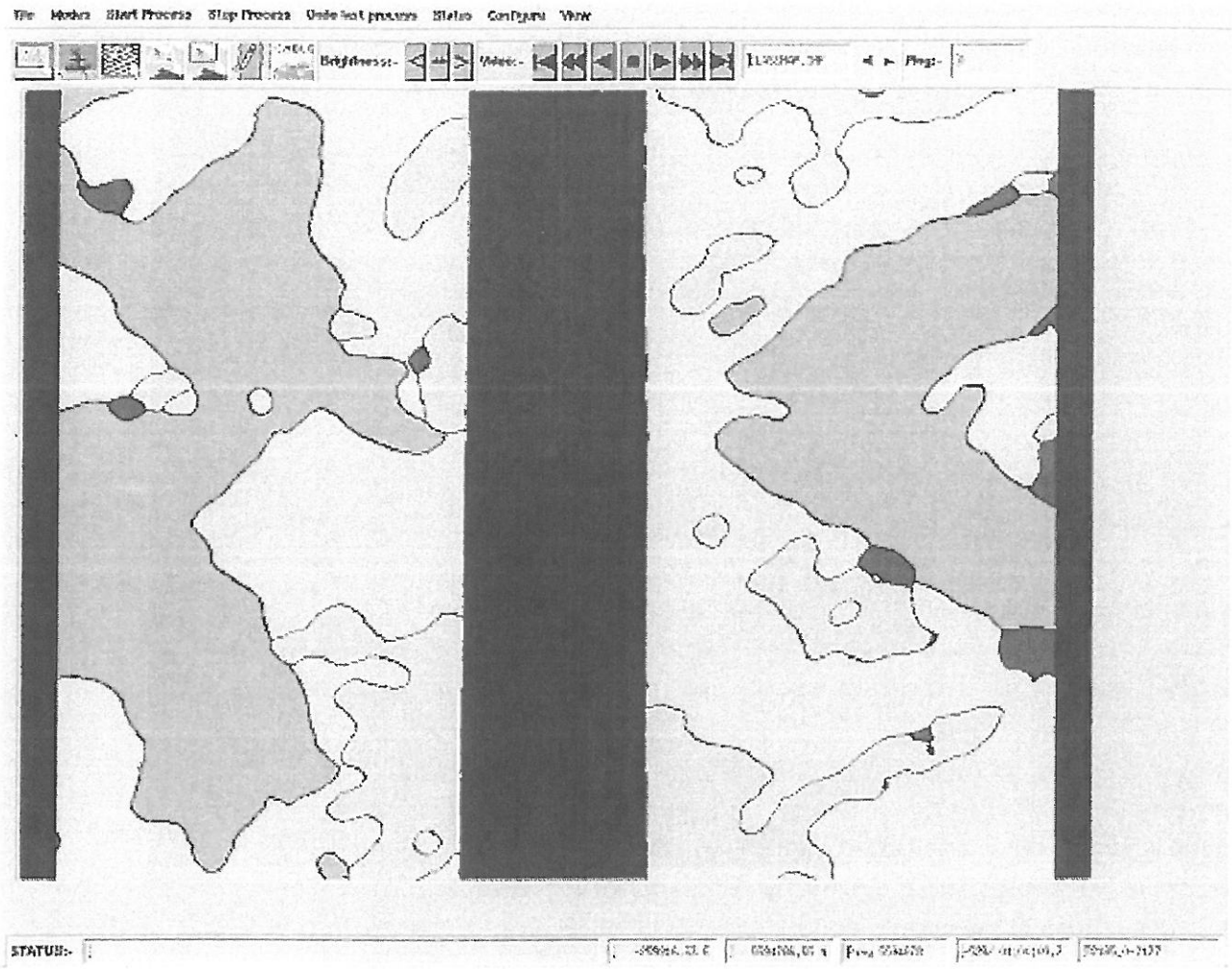

Fig. 21.5. Sidescan sonar sediment classification using image processing algorithms on the data of Fig. 21.4. The four different grayscales correspond to a classification of the sea bed, using texture image processing of sidescan sonar, from darkest gray to lightest, as follows: gravel, sand, muddy sand, mud. The left and right panels correspond to the geometries described in the caption for Fig. 21.4. (Image provided using the Classiphi™ system courtesy of QinetiQ Ltd.)

are termed sand (2 mm $> 2a >$ 0.0625 mm), silt (0.0625 mm $> 2a >$ 0.0039 mm), and clay (0.0039 mm $> 2a$). However the "effective roughness" of a surface does not depend only on the physical size of the surface relief or grains, but also on the wavelength of the radiation used to resolve them. The high spatial resolution imparted by VHF acoustics, compared to that available at lower frequencies, means that fine roughness features become resolvable. Consider when the Rayleigh criterion is used to determine the roughness of the surface, with respect to the incident acoustic wave number (k). It is based on the Rayleigh parameter, $R_a = kh \sin\theta_g$ where h is the rms height of bed ripples with respect to a mean plane, and θ_g is the source angle with respect to grazing incidence. The Rayleigh

criterion states that if $R_a < \pi/4$ then the surface is regarded as smooth, whereas if $R_a > \pi/4$ then the surface is regarded as rough. It is clear that the wavelength of interest at VHF frequencies would start to be comparable with the roughness dimension of the sediment (from shell-size at 200 kHz to sand-grain size at 1 MHz). For a plane sediment surface insonified with VHF acoustics, surfaces made of gravel would start to look very rough. It is, however, interesting to note that sediments with finer grains (sand, mud, silt, and clay) would still fall below the Rayleigh criterion. In reality the sediment always contain some surface relief, so that the contribution to roughness from this would also need to be taken into account. In principle these surfaces exceed the Rayleigh criterion, and the surface should be treated as a rough surface. This is as would be expected for decreasing wavelength.

Close inspection of the sidescan sonar image provided in Fig. 21.4 reveals that the texture (highlights and shadows) is directly related to the undulations on the sediment, so that the front face of the ripple gives a high backscatter which gradually reduces as the local grazing angle decreases, with a shadow region behind the ripple. Whilst it is true that the surface would look rough if the insonification were over a number of ripples, hence giving incoherent backscatter, in the case where a short pulse length is used (which is most often the case at VHF) the surface spectrum must be truncated to take account of this effect. Brothers *et al.* (1999) have applied this truncation scheme to the composite roughness model and made good comparisons with experimental data. Their scheme was applied to both short pulse length and pulse compressed wideband signal. As the insonified area decreases it must, by definition, remove some of the lower frequency components from the surface spectrum. This must be taken into account in modeling or when conducting experiments, if representative scattering levels are to be achieved. If this argument is taken to its extreme, then the insonified area becomes a single point on the surface, which is effectively smooth, and hence the scattered levels would be a function of the angle of the facet and the reflection coefficient.

In summary, VHF scattering has the potential to offer acoustical oceanography new tools for exploration of the sea floor. As a first example, given that VHF beams might only penetrate a few centimeters into the seabed, comparison of VHF and lower frequency scatter might allow discrimination between information on the water/bed interface and that which scatters from deeper in the seabed. This point will be expanded upon in the following section with discussion of a commercial device. Second, consider that at lower frequencies sediments have been modeled as a frame structure (Stoll, 1974) based on the Biot theory. If this theory holds at high frequencies, then it is possible that resonances would

be observed at frequencies much lower than would be expected for the individual grain resonances. The ability to observe any such resonance will depend on the amount of damping which, if high, would suppress any effect. The question of whether models will be able accurately to predict sound speed in sediment is raised by the suggestion that the apparent velocity of sound in the sediment might decrease as the frequency rises above 350 kHz (an effect which also appears to happen in artificial seabeds comprising glass beads). Because each sediment grain (or glass bead) is not necessarily connected to its neighbors, the energy which passes though the sediment alone has to take a complex route. This increases the path length, thus giving the impression of reduced velocity at lower velocity. Finally, there is seldom a clear distinction between pure seabed and the water column. Boreholes, gas bubbles in sediment, and gas bladders on weeds, shells, and other fauna and flora all have the potential to scatter VHF signals significantly, perhaps even enough to swamp the background level that would normally be seen from the sediment alone. The next section, however, details more subtle phenomena which produce a finite transition zone between seabed and water column.

21.5 Flow-related processes in the bed/water column transition zone

The transition region between two media always has the potential to be complicated (see, for example, Section 21.6). The acoustical implications of the boundary between a well-defined seabed and the water column were discussed in Section 21.4, from a viewpoint that, even with such "clutter" as shells and weed on the seabed or bubbles beneath it, the two regions could to a degree be well-defined because those items tend to present discrete scatterers to VHF signals. This section discusses the more subtle ectopia which characterize the transition between the seabed and the water column.

The most obvious of these features which subtly blend the seabed into the water column, is the suspended particulate matter. Much of this first rises from some bed (sea, river, or estuary) as the result of turbulence, tidal action, waves, etc. and then tends to settle back towards it under gravity (Fig. 21.6). In still water there would therefore be a concentration gradient of such matter, it becoming less concentrated as one moves away from the seabed, a tendency which is reduced by turbulence, etc. The importance of such "sediment in transport" has been recognized for thousands of years: its deposition during the annual flooding of the Nile determined the fertility of the land, a dominant feature in the religion, culture, and politics of Egypt from 4500 BC until the last century.

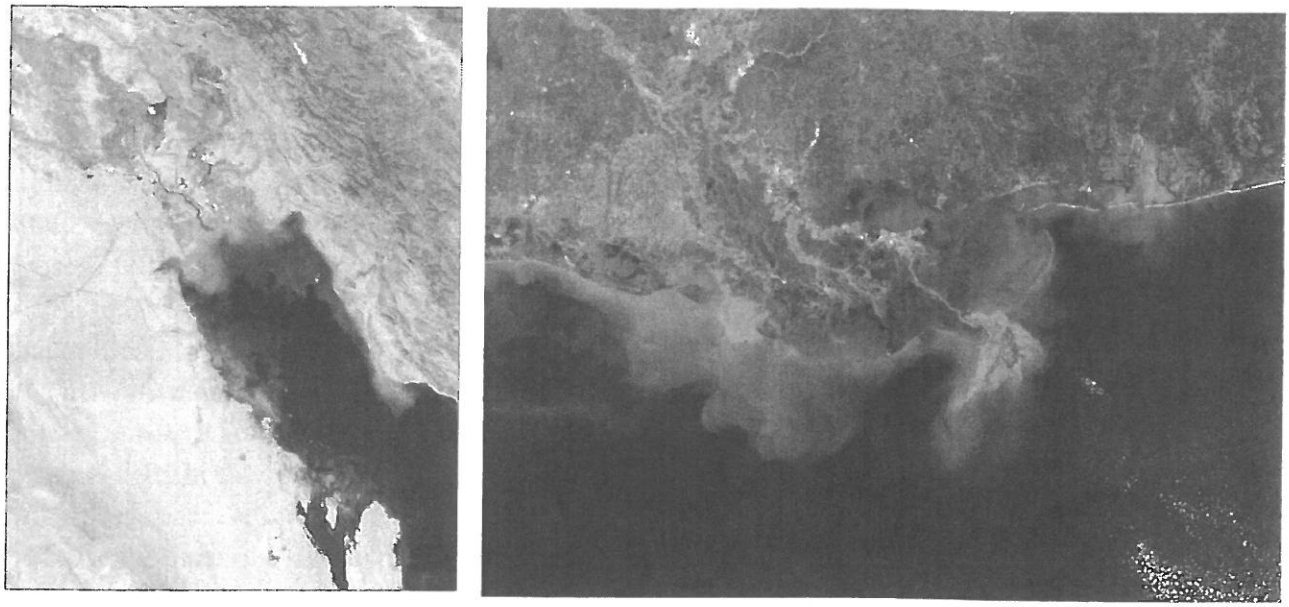

(*a*) (*b*)

Fig. 21.6. True-color satellite images (from the Moderate Resolution Imaging Spectroradiometer MODIS carried by NASA) of sediment carried by rivers into the sea. (*a*) As a result of flooding by the confluence of the Tigris and Euphrates Rivers (at center), the sediment-laden waters of the Persian Gulf (November 1, 2001) appear light brown where they enter the northern end of the Persian Gulf and then gradually dissipate into turquoise swirls as they drift southward. (Image courtesy Jacques Descloitres, MODIS Land Rapid Response Team at NASA GSFC.) (*b*) The Mississippi River carries roughly 550 million metric tonnes of sediment into the Gulf of Mexico each year. Here (March 5, 2001 at 10:55 am local time) the murky brown water of the Mississippi mixes with the dark blue water of the Gulf two days after a rainstorm. The river brings enough sediment from its 3 250 000 square km (1 250 000 square miles) basin to extend the coast of Louisiana 91 m (300 ft) each year. (Image courtesy Liam Gumley, Space Science and Engineering Center, University of Wisconsin-Madison and the MODIS science team.) Source: NMASA, reproduced with the permission of the Lunar and Planetary Institute. (See colour plate section.)

Today the presence of suspended sediment reduces the ability of active sonar systems to detect mines and torpedoes (the sonar equivalent of the effect of fog on car headlamps). Conversely, the acoustic scattering and absorption it produces can be used to monitor this environmentally important feature.

Because typical particle diameters $2a$ are in the range 0.1–100 μm, such suspensions scatter most strongly at VHF. Up to $ka \sim 1$ (which for $c = 1500$ m s^{-1} occurs at frequency f of 2.4 MHz for $a = 100$ μm; and at higher frequencies for the smaller particles), Rayleigh scattering occurs: the scattered power increases as both particle size and frequency increase (eventually taking an oscillatory form in the geometric regime

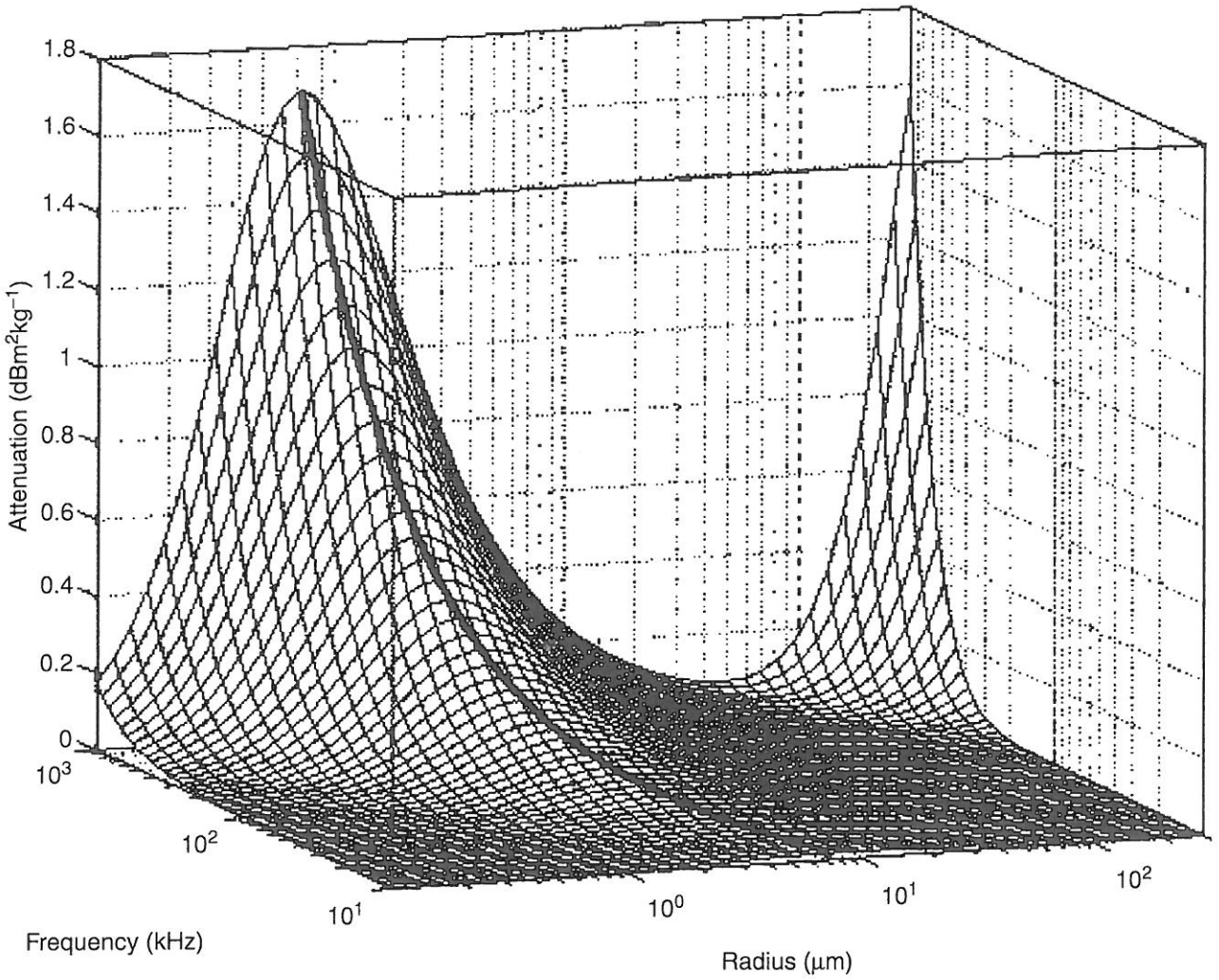

Fig. 21.7. Plot of acoustic attenuation constant dB m^{-1} (normalized to mass concentration kg m^{-3}) for suspensions of quartz spheres in sea water. The bold line tracks the local maximum of the absorption contribution. (Image courtesy S. D. Richards.)

where $a/\lambda \gtrsim 1$). The surface plotted in Fig. 21.7 is still undergoing this Rayleigh-regime growth as it passes through the rear right corner (i.e., large-radius, high-frequency limits) of the figure. Within this Rayleigh regime, at a fixed frequency the cross-sectional "target" area πa^2 "seen" by the ultrasonic beam increases quadratically with radius.

However, Fig. 21.7 plots, not just the scatter, but the attenuation. There is a second contributing factor to this, namely the acoustic absorption. This occurs because the density of the solid is different from that of the water. As a result, when an acoustic wave propagates through the water (the particle velocity reversing every half-cycle), the motion of the latter is not in phase with that of the particles. There is net flow around the particle, and viscous losses occur in a viscous shear boundary layer which extends around each particle to a "skin depth" of about

$\sqrt{\eta/\pi\rho f}$ (i.e., O[1 micron] in water at 500 kHz), for frequency f in a liquid of density ρ and shear viscosity η. The contribution of these losses to attenuation exhibits a local maximum for fixed frequency (see the bold line in Fig. 21.7). This is because very small particles move almost in phase with the fluid, whilst very large particles hardly move at all. Hence both activities are almost loss-less. Maximum absorption losses occur when the particle radius is a comparable size with the skin depth for shear waves, resulting in a maximum phase difference between the motion of the water and that of the particle.

To use either scatter, absorption, or both to measure suspended sediments at sea requires development, testing, and calibration of those instruments in the laboratory. Because of this, measurement of backscatter from suspended sediment has been far simpler than use of absorption, because the backscattered signal is so much easier to detect in controlled laboratory systems than the absorption loss. Whilst the latter can be significant in the ocean, where propagation lengths of km or more are used (Richards and Leighton, 2001), the finite size of laboratories makes it difficult to generate controlled, sizeable absorption losses. This difficulty increases as the acoustic frequency decreases, because the absorption is greater at higher frequencies. Hence whilst Urick (1948) compared absorption loss due to kaolin and fine sand at 1–15 MHz with theory for spherical particles, it is only in recent years that the dilute suspensions typical of the ocean have been compared with predictions of an appropriate theory (of, for example, non-spherical particles) at O[100 kHz] (Richards *et al.*, 2003). This has allowed feasibility studies of how absorption might be used to monitor mass flux by large rivers (Richards and Leighton, 2001). Crucially the technique would allow the measurement to be made right across the length of the river, averaging over 100 m or more, to monitor the entire mass flux.

In contrast, whilst the stronger laboratory signal allowed systems based on particulate backscatter to be developed more easily, they have been restricted to local measurements, with small (ml) sample volumes O[1 m] from the sensor. This is because, as the magnitude of the relevant effect (i.e., backscatter or attenuation) illustrated by Fig. 21.7 suggests, scatter systems should typically exploit higher frequencies (typically O[1 MHz]) than do absorption systems (O[100 kHz]). Clear sea water has an absorption coefficient of ~0.5 dB/m at 1 MHz (depending on temperature, salinity, pH etc.), so 100 m of river mouth would degrade the two-pass backscattered signal by up to 100 dB. In contrast, the ~3 dB degradation seen in a one-pass bistatic absorption device (sea water absorbing at ~0.03 dB/m at 100 kHz) would provide the base-line absorption against which the enhanced absorption due to particles would need to be observed (Leighton, 1998).

One might ask why the backscatter technique does not exploit the O[100 kHz] frequencies and thereby extend the range over which it might measure. The problem is that, as the frequency decreases in this range, the scattering strength becomes small because $ka \ll 1$ (Fig. 21.7). If however the process of estimating particle sizes and concentrations from backscatter (inversion) is restricted to the MHz range, an additional benefit accrues. Inversion requires calculation of the acoustic attenuation of the beam as it passes through the particulate suspension, and the accuracy with which the contribution of particulate absorption needs to be described need not be too exacting. Figure 21.7 shows that scatter, rather than absorption, dominates attenuation at 1 MHz for populations of large particles (e.g., 50–100 microns radius), such as sand. The effects on the predicted attenuation resulting from a simplified expression for the particulate absorption are small (Holdaway *et al.*, 1999). If however micron-sized particles dominate the populations (as in fine clay and silt), then the contribution of absorption becomes more important, and calculation of their contribution to attenuation might require such complexities as consideration of particle shape (Richards *et al.*, 2003).

To add perspective however, whilst absorption techniques alone offer the prospect of measuring over long paths without using multiple sensors, they have yet to be used in the field to measure sediment in transport. In contrast, whilst scatter techniques are not as widespread as optical ones, they are commercially available, and are becoming increasingly accepted as valuable both in their own right, and as providing a useful synergy with optical and conventional techniques (which include bottle/pumped sampling; laser diffraction; optical backscatter; spectral reflectance; and the optical transmittance and absorption of water, usually as measured at several wavelengths using the "transmissometer") (Holdaway *et al.*, 1999; Thorne and Haynes, 2002). Whilst the backscatter technique lacks the ability to integrate spatially over large volumes without multiple hardware, the compensation is that the suspended sediment can be measured with high spatial resolution. The sampling volumes are formed by dividing the returned signal into time bins. The time limits of each bin demarcate the start and end ranges respectively of the volume sample. For the AquaScat™ (a commercial acoustic backscatter sensor) these volume elements have lengths of 10 mm (with 5 mm and 2.5 mm options) at ranges of typically 1 m. The cross-sectional area of the volume element is controlled by the beamwidth (the AquaScat™-3dB half beamwidth being 1.4°–0.9° in the range 3–5 MHz, assuming a 10 mm diameter disk transducer).

However, the small wavelength also means the bed profile can be measured and even imaged, in the manner described in Section 21.4. The AquaScat™ also has a "long range" (O[10 m]) mode, with volume

elements 20 mm–160 mm long, capable of measuring morphology (e.g., seabed ripples, Section 21.4). In addition to small sample volumes and the ability to measure morphology (with images of up to 10–30 m^2; Thorne and Haynes, 2002), the O[MHz] frequencies employed in backscatter offer a third advantages over the O[100 kHz] range. Because they are more strongly attenuated by the sediment than by range, the higher frequency backscatter in principle contains more information about the surface (uncluttered by returns from depth) than the lower frequencies (see Section 21.4). Hence most of the information in the returned signal comes for the water/bed interface, and not from the depths of the seabed, and the "blindness" of the high frequencies to the depths of the seabed simplifies their interpretation when used as an interface sensor.

Not only can backscatter measure suspended sediments and bed profile simultaneously, VHF systems in the bed/water transition zone can also measure flow. Absorption systems are relatively insensitive to flow and turbulence, which is beneficial in that it gives the assurance that flow-induced losses are not being interpreted as indicating the presence of spurious particles (Richards *et al.*, 2003). However, this also means that they would not make good sensors for flow. Backscatter systems are however sensitive to flow and turbulence, and can be used to monitor it, providing there is none of the above ambiguity mentioned above. The Coherent Doppler Velocity Profiler (CDVP) exploits the effect of Doppler shift on the phase coherence between consecutive backscattered pulses to determine the component of flow velocity in the direction of the beam axis. Alternatively, the Cross-Correlation Velocity Profiler (CCVP) examines the temporal coherence in the suspension as it is advected, for example, through two vertical ultrasound beams, transmitted by a pair of closely spaced, horizontally aligned transducers. If the backscattered signal is divided into time bins, each bin represents data from a further range than the bin previously. Cross-correlating the returns from each emitter allows identification of the time interval it takes for the suspension to advect from the first beam to the second, allowing the velocity profile to be determined (Thorne and Haynes, 2002).

The changeover between Sections 21.4 and 21.5 introduced a variety of features which can make up the transition zone between the bed and the water. Whether they are associated with biology, trapped in sediment, or present in the form of free gas, a relatively small number of bubbles can contribute so much to acoustic scatter and absorption, that sensors of suspended sediment based on either system can be compromised (Richards and Leighton, 2001). However the strength of bubble scatter can be exploited, for example by using the bubbles themselves as tracers for flow (Thorpe, 1982). This is because, notwithstanding the ability of bubbles associated with the bed/water interface to scatter strongly, in

most coastal waters the greatest acoustical effects are generated by those bubbles which are entrained at the top of the water column and move through it. The VHF effects of these bubbles will be the topic of the next section.

21.6 Bubbles

Both the acoustical and near-shore aspects of VHF bubble effects in coastal waters are fascinating and, to a large part, undiscovered. Bubbles are formed through a variety of mechanisms in the oceans, ranging from methane seeps to plunging breakers. In the coastal waters of this chapter, mechanisms which are less important in deeper water may become more important. These include the production of bubbles by biology and the flux of gas in sediment which is exposed at low tide. Most impressive, however, and most potent acoustically, are the effects of coastal breakers (Fig. 21.8), which can generate huge void fractions (the proportion of a sample of bubbly water which, by volume, is free gas) see Chapter 6.

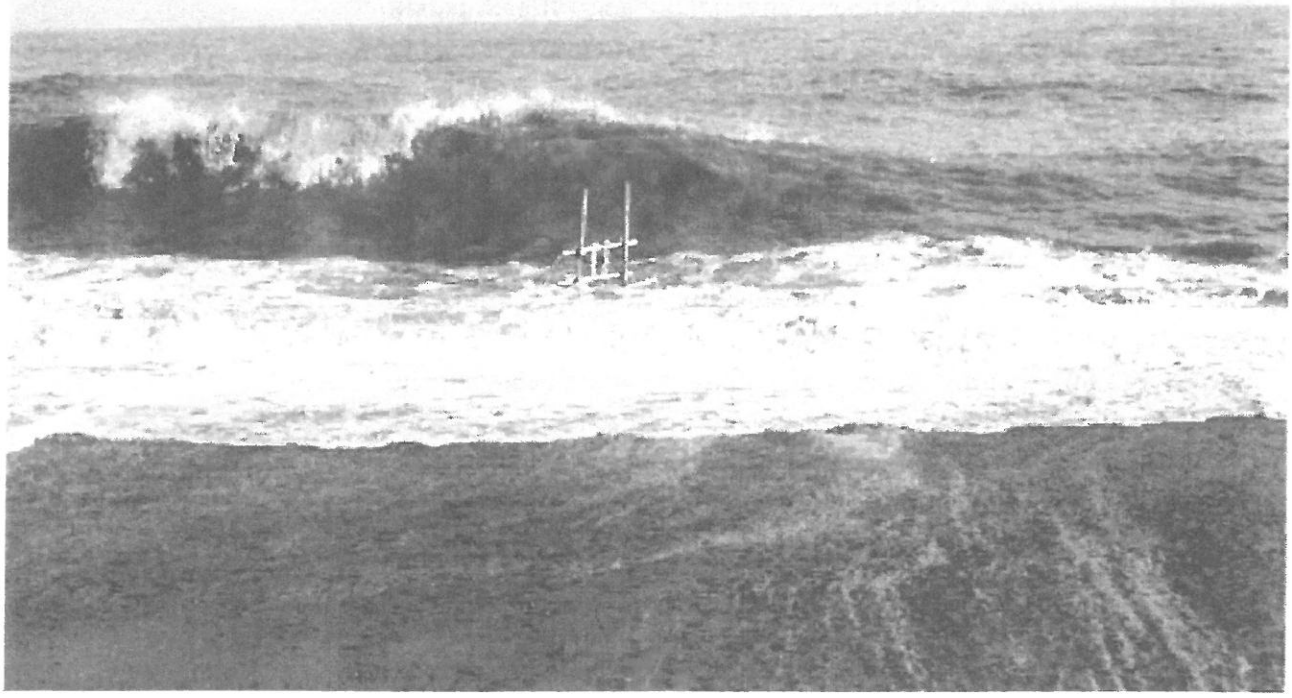

Fig. 21.8. A 10 ft wave breaks over a combination-frequency bubble detector, which can be seen as a small black circle strapped between the cross-bars on the scaffolding. The plunging breakers on the water's edge were consistently far more active than any of the waves further from shore (Leighton *et al.*, 1996).

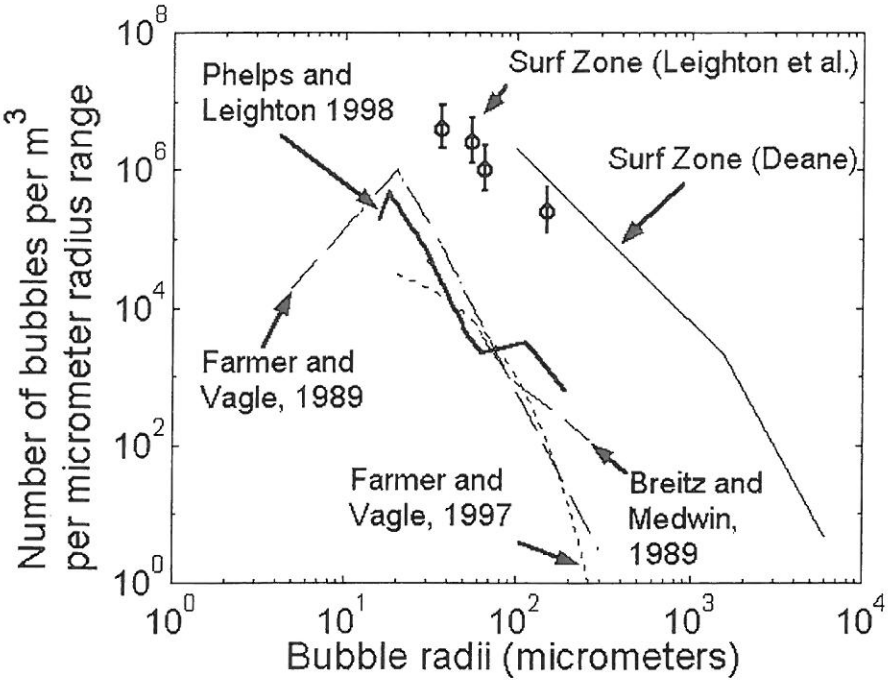

Fig. 21.9. The number of bubbles per cubic meter per micrometer increment of radius ($n(R_0)$ – see text for details), shown for a range of oceanic bubble populations, both in the surf zone (Leighton *et al.* 1996 *c*, Deane 1997 *d*) and out of it (Farmer and Vagle 1989 *a* and 1997 *b*, Breitz and Medwin 1989 *b*; Phelps and Leighton 1998 *c*). Labels *a–d* relate to experimental techniques described in Fig. 21.10, as explained in the text (from Leighton *et al.*, 2001).

Bubbles can enter into the VHF aspect of coastal acoustics in two ways. The first is through the pulsation resonance frequency f_0 of small bubbles. As discussed in Chapter 6, f_0 varies inversely with bubble size, so long as surface tension effects are neglected. This is valid down to a bubble radius of $R_0 \sim 7$ microns, where the inverse relationship fails because, for air bubbles in "dirty" ocean water (Thorpe, 1982) having an assumed surface tension $\sigma = 3.6 \times 10^{-2}$ N m^{-1}, surface tension contributes to the bubble gas pressure a component $p_\sigma = 2\sigma/R_0$ equal to 0.1 atm (Leighton, 1994). For air bubbles of 7 microns radius under 1 atm, f_0 is about 400 kHz. Hence the transition from the HF (high frequency) to the VHF regime is very interesting in bubble acoustics. VHF values of f_0 represent the region where surface tension on the bubble, which we do not know well, becomes important. This in turn affects the validity of our inversions of acoustical data to estimate bubble numbers. Moreover, having obtained these bubble counts, our estimates of, for example, atmosphere/ocean mass flux (which for atmospheric carbon alone may exceed 10^9 tonnes per year globally) are compromised by uncertainties in surface tension. Furthermore, the VHF range for f_0 also represents the lower limit where bubble population estimates have been made in the ocean, as will now be shown.

Do such small bubbles, resonant at frequencies greater than 200 kHz, exist in the ocean? Figure 21.9 plots a histogram of the bubble population, as measured in the oceans by various researchers (a small sample of the data sets available). The abscissa shows the bubble radius divided into bin sizes of 1 micron width, and $n(R_0)$ plots the number

of bubbles per cubic meter of sea water contained within that bin. One extraordinary feature illustrated by Fig. 21.9 echoes the sentiment at the start of this chapter, that the waters closest to us are in some respects perhaps the least explored. The two "surf zone" data sets in Fig. 21.9 represent only a handful taken close to shore, in contrast to a multitude of data sets taken further from land (some of which are shown in Fig. 21.9). Note also the scarcity of small-bubble data: the smallest bubble radius shown in Fig. 21.9 corresponds to a bubble resonance frequency of 200 kHz; and the smallest taken to the authors' knowledge had a 9 micron radius, corresponding to a bubble resonance of 360 kHz (see Leighton *et al.*, 2001 and pp. 235–241 of that volume). Hence the lower limits of the VHF range represent the beginning of the "undiscovered" region of oceanic bubble size distribution, where data are scarce and, as discussed above, surface tension effects can dominate.

The second way in which bubbles can enter into the VHF aspect of coastal acoustics is through the combination-frequency techniques which are used by some researchers to obtain $n(R_0)$. Figure 21.10 illustrates the

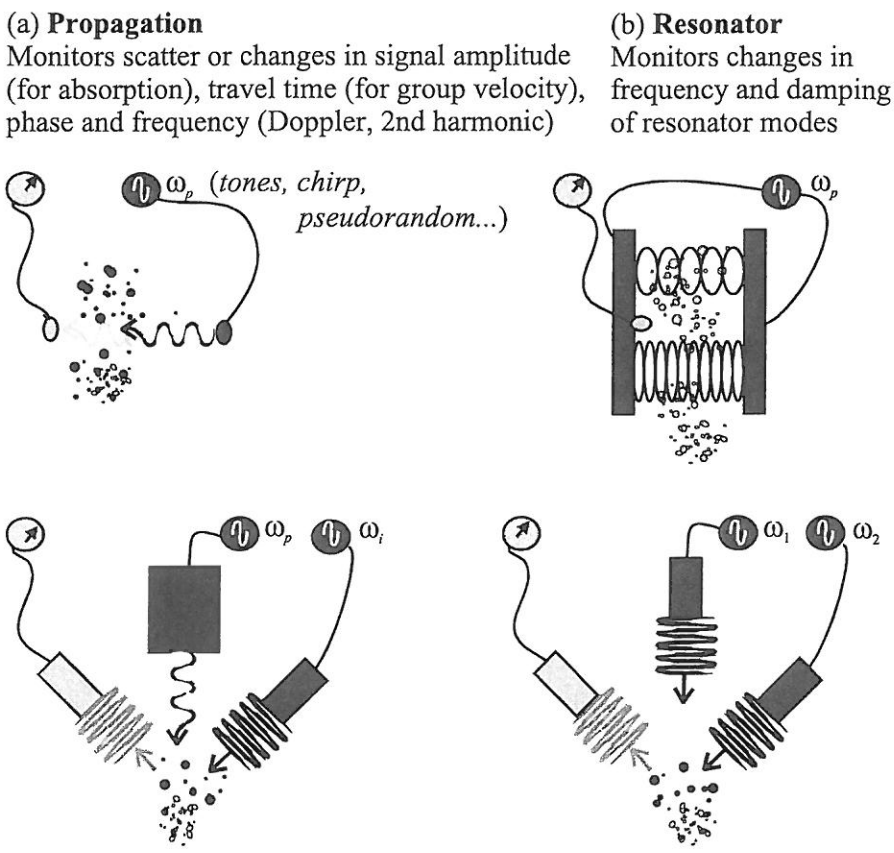

Fig. 21.10. The four main families of active acoustical techniques for obtaining the bubble size distribution, $n(R_0)$. Transmitters and their waveforms are shown in dark gray; receivers and received waveforms are shown in light gray. (*a*) Propagation techniques; (*b*) Resonator method; Also shown are bubble-mediated generation of (*c*) modulation frequencies and (*d*) combination frequencies. Note that *n* and *m* correspond to non-zero integers. (From Leighton, http://www.isvr.soton.ac.uk/fdag/UAUA/INDEX.HTM)

four broad categories of acoustical techniques for measuring $n(R_0)$, the dark gray corresponding to transmitters and their waveforms, and the light gray corresponding to receivers and received waveforms. Methods *a–c* all transmit a signal which is figuratively indicated by ω_p, the "pump" signal, which in general terms is meant to drive bubbles into pulsation and elicit the strongest response from those resonant at ω_p. Implementation of this technique, however, needs to take into account the fact that other bubbles (e.g., having radii much larger than the radius which is resonant with ω_p) might also contribute to some measured effects, such as attenuation at ω_p (Commander and McDonald, 1991): such big bubbles may not pulsate to large amplitude when driven at ω_p, but they can nevertheless scatter strongly because they represent physically large targets of gas in water. To avoid such ambiguities, the tendency is to move to effects which such large "inert" bubbles cannot produce, which often means exploiting the non-linearities which bubbles can generate when they pulsate at high amplitudes. Since high amplitude pulsation usually occurs in bubbles having radii which are close to resonance at ω_p, the non-linear effect can be taken as diagnosing the presence of resonant bubbles. One example is the non-linear generation of signals $2\omega_p$ by bubbles insonified at ω_p (Ostrovsky *et al.*, 2003). The generation of effects at $2\omega_p$ can readily be appreciated if the non-linear fluid element in (21.8) is the bubble. If, however, it represents, say, turbulence, then one can understand how even this signal may be unreliable if used to count bubbles under a turbulent breaking wave, if the sensor interprets all the $2\omega_p$ as being generated by near-resonant bubbles. Similar comments apply to the techniques shown in Figs. 21.10 *c* and *d*, where non-linear effects such as turbulence, as well as bubbles, may generate signals at $\omega_1 \pm \omega_2$, $\omega_i \pm \omega_p$, $\omega_i \pm 2\omega_p$, etc. All these are VHF issues, since if (as shown earlier) there are enough small bubbles in the ocean for ω_p to be in the VHF range, certain harmonics of it will be.

The techniques in Figs. 21.10 *c* and *d* are, however, VHF issues for another reason. As with *a*, *b*, in the modulation frequency method and (*c*) a pump signal is emitted in order to drive the bubble to pulsate. However a VHF "imaging" signal (at ω_i) is then scattered off the pulsating bubble: on the timescale of the ω_i signal, the wall of a bubble which is pulsating at ω_p is moving relatively slowly, and so the amplitude of the scattered ω_i is modulated on the slower timescale of ω_p (as the bubble expands and contracts; Fig. 21.11 *a*). This is interpreted in the spectra as the appearance of energy at $\omega_i \pm \omega_p$ in addition to the original ω_i signal (an alternative and equivalent description for the generation of these signals can be seen in (21.9)). If the pulsation of the bubble has a second harmonic component, signals at $\omega_i \pm 2\omega_p$ will also be detected, and so on (Ostrovsky *et al.*, 2003). Noting that in principle such signals

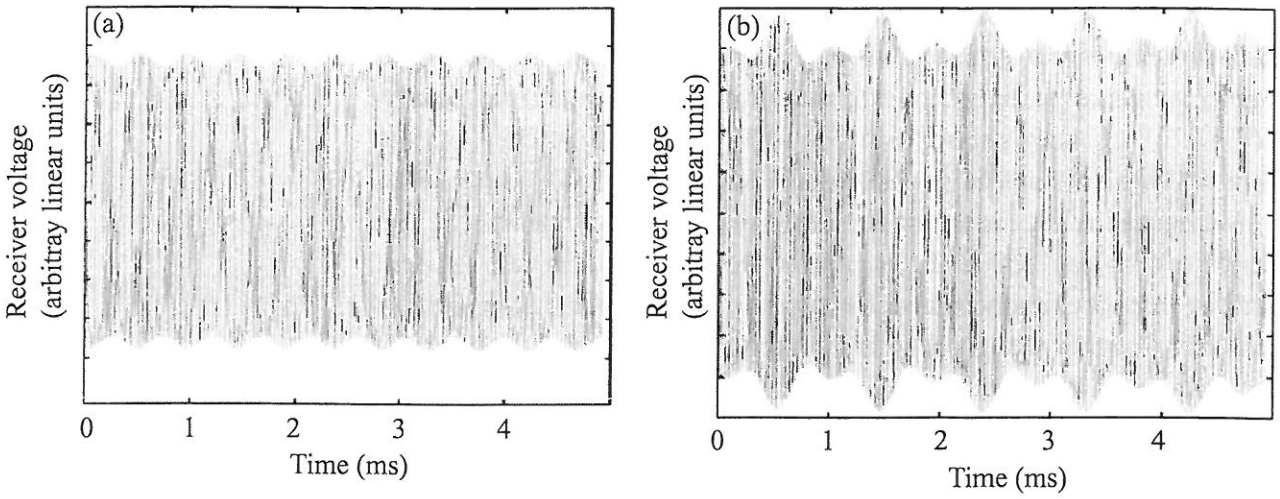

Fig. 21.11. Imaging signal modulated at (*a*) ω_p and (*b*) $\omega_p/2$. The period of the imaging signal is so short on the timescale of this plot that its sinusoid plots closely enough to appear as a solid black entity (Leighton, 1994).

could also be produced by any other source of non-linearity which could be described by power-series of (21.8), Leighton *et al.* (1996) exploited a signal which could not be generated through (21.8), specifically the generation of signals at $\omega_i \pm \omega_p/2$. These can also be visualized as scattering of the imaging signal by a target whose strength varies on a much slower timescale, as described above, only here the slow timescale corresponds to the subharmonic of the pump frequency (Fig. 21.11*b*). The shape mode on a bubble wall which requires the lowest threshold driving pressure to excite is the Faraday wave (Fig. 21.12), which oscillates at the subharmonic and was shown to be the source of the emission at $\omega_i \pm \omega_p/2$ (Phelps and Leighton, 1996, 1997).

Unlike the other techniques, the combination frequency method (Fig. 21.10*d*) does not emit a pump signal to drive the bubble into pulsation. Instead, two VHF signals (ω_1, ω_2) are transmitted into the water, and signals generated at $\omega_1 - \omega_2$ are taken to reflect the presence of bubbles resonant at that difference frequency (Didenkulov *et al.*, 2001; Ostrovsky *et al.*, 2003).

In the caption to Fig. 21.9, each of the bubble size data sets is labeled with a letter, *a–d*, to indicate which method (of Figs. 21.10*a–d*) was used to make the measurement.

In summary therefore, VHF enters bubble acoustics through the high natural frequencies of the large number of small bubbles prevalent in coastal waters, and consequently through the high value taken by ω_p and related signals ($2\omega_p$, $\omega_i \pm \omega_p$, $\omega_i \pm 2\omega_p$, etc.) used in determining the bubble numbers. In addition, two types of active acoustical techniques (Figs. 21.10*c* and *d*) transmit VHF signals (ω_1, ω_2, ω_i) into the water,

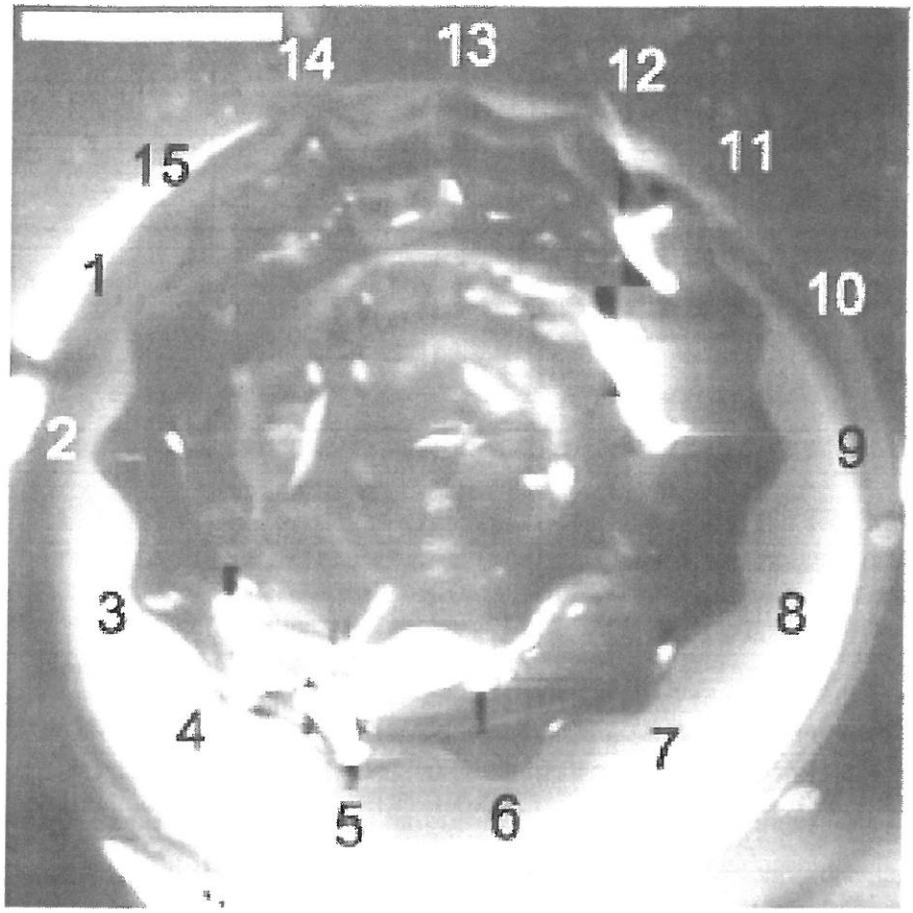

Fig. 21.12. A Faraday wave is stimulated on the wall of a pulsating bubble, driven at 1.29 kHz. The white line at the top of the figure is a 2 mm length scale bar. Just as the pulsation can be described as a perturbation on the bubble wall corresponding to the zero-order spherical harmonic, so this Faraday wave corresponds to its perturbation by a spherical harmonic of order 15 (as can be seen by counting the peaks and troughs on the bubble's wall). (Photograph: P. R. Birkin, T. G. Leighton and Y. E. Watson.)

not to drive the bubbles into pulsation, but rather to enable them to be detected through processes which may be described as non-linear.

21.7 Conclusions

Space limitations have meant that only a few VHF acoustical issues in coastal waters have been covered in this chapter, and those not to great depth. Additional issues are mentioned below.

VHF acoustic signals have sufficiently small wavelengths to allow the acoustic scatter from many features to be understood by analogy to optics. Both the top and bottom of the water column can be reflective. Figure 21.13 illustrates how, as a result of this, an observer will receive a sound field as if the reverberation were generated by images (with appropriate time/phase delays). The case when the observer is itself the source of sound is particularly fascinating. A sound source in idealized wedge-shaped coastal waters can "perceive" image sources; one can, for example, imagine how a single cetacean might see this as a ring of "twins." Whilst of course an intelligent creature might recognize such reverberation for what it is, other sound sources may not. For a bubble, such reverberation will alter the natural frequency and damping expected

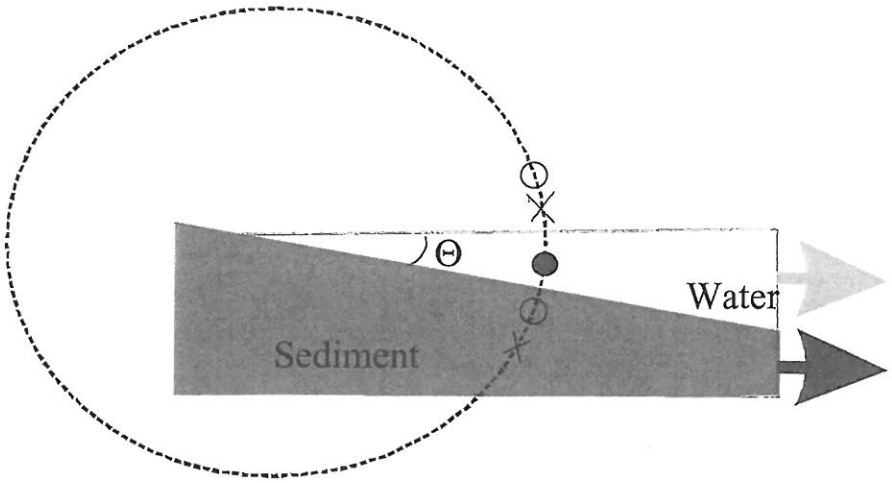

Fig. 21.13. If a coastal zone can be approximated by a wedge shape of ocean, with a bottom which reflects acoustic pressure waves with no phase change, and an air/water interface which reflects them with π phase change, then the net sound field built up in the water by an object (•) emitting sound will be that which would be produced were the object in free-field, and sound were in addition emitted by image sources either in phase (○) with the original source, or in antiphase (×). The sediment and atmosphere boundaries of the water column being flat acoustic mirrors in this model, in the 2D plane passing vertically through the source these images will be distributed around the circle shown by the dashed line. The first few image sources are shown (○,×). For certain wedge angles Θ (such as the 15° used for Fig. 21.14) the sources map on to discrete sites on the dashed circle.

in free-field conditions (see Chapter 6), as illustrated in Fig. 21.14 for the ideal wedge of Fig. 21.13 (Leighton *et al.*, 2002).

Of course most coastal regions do not resemble the flat-sided wedge of Fig. 21.13, but these complications make the coastal region even more fascinating for sensors of VHF acoustics. The optical equivalent would be stranger than a carnival "hall of mirrors," its floor covered by a fluctuating "dry-ice fog" (the optical equivalent of suspensed sediment particles), its wedge-shape complicated by ripples on the mirrored floor. Its ceiling would be an undulating, highly reflecting mirror, in some places focusing the sound in moving "hot spots" within the water column and floor, and in other places producing areas of dark, absorbing bubble clouds covered with a bright speckle of resonant bubble scatterers. Imagine those clouds being explosively generated by a breaking wave, then spreading over time.

Since most VHF acoustics intend to deploy discrete beams in a monostatic or bistatic scenario, the optical equivalent might involve one or more people with flashlights in this otherwise dark "hall of mirrors." As the frequency increases to the upper VHF, the absorption reduces the amplitude transmitted to, and scattered back from, a distance away. In

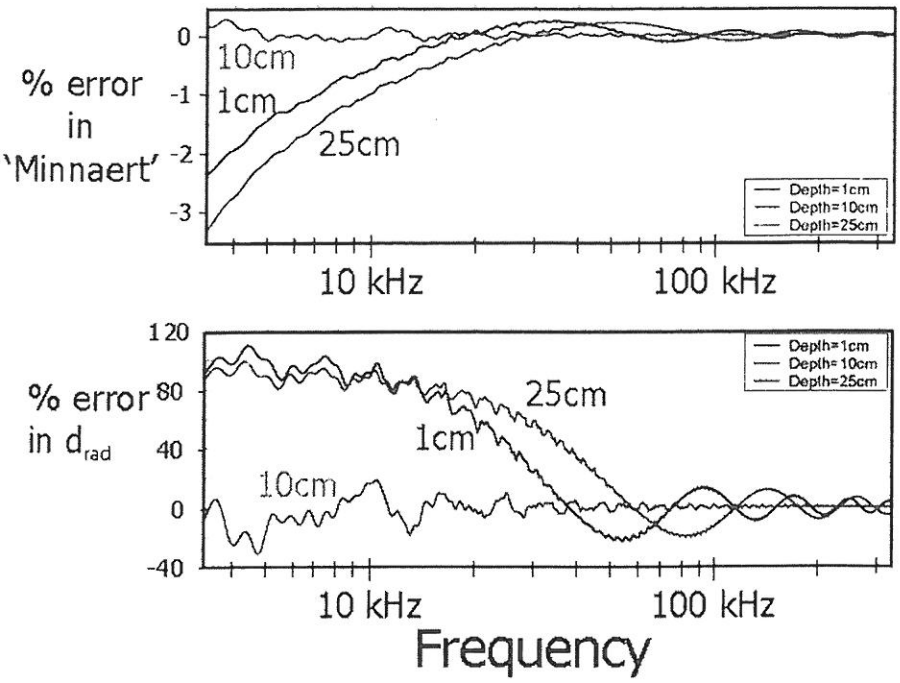

Fig. 21.14. The percentage error between the actual natural frequency of a bubble and the radiation damping constant, respectively, if the free-field formulations of Minnaert and Devin are used in the 15° wedge shown in Fig. 21.13. The result is shown for three bubble depths, for a bubble situation 1 m from the water's edge (where the water depth is 26 cm). (Figure by T. G. Leighton and P. R. White.) (See colour plate section.)

the monostatic optical equivalent it would be as if the flashlight emitted a dim red light in the carnival hall of mirrors; when, to compensate for this, the brightness of the flashlight is increased, blue new colors might be generated (the optical production of second-harmonic production described in Section 21.2, though of course the frequencies of blue light in the optical analog are not twice that of red).

21.8 The future

The move into research at VHF frequencies, over 200 kHz, offers the excitement of a transition into the "unknown." With respect to bubbles, sediments, and a range of other oceanographic phenomena, whilst we cannot say that all is well-understood at frequencies below 200 kHz, we are sure that the VHF regime offers the excitement of discovery and the potential for new acoustical tools. This is especially so in coastal waters which, whilst being the most explored by our vessels, are also the least understood acoustically.